



Since January 2020 Elsevier has created a COVID-19 resource centre with free information in English and Mandarin on the novel coronavirus COVID-19. The COVID-19 resource centre is hosted on Elsevier Connect, the company's public news and information website.

Elsevier hereby grants permission to make all its COVID-19-related research that is available on the COVID-19 resource centre - including this research content - immediately available in PubMed Central and other publicly funded repositories, such as the WHO COVID database with rights for unrestricted research re-use and analyses in any form or by any means with acknowledgement of the original source. These permissions are granted for free by Elsevier for as long as the COVID-19 resource centre remains active.



## ALG-097111, a potent and selective SARS-CoV-2 3-chymotrypsin-like cysteine protease inhibitor exhibits *in vivo* efficacy in a Syrian Hamster model



Koen Vanduyck<sup>a,\*</sup>, Rana Abdelnabi<sup>d</sup>, Kusum Gupta<sup>b</sup>, Dirk Jochmans<sup>d</sup>, Andreas Jekle<sup>b</sup>, Jerome Deval<sup>b</sup>, Dinah Misner<sup>b</sup>, Dorothee Bardiot<sup>e</sup>, Caroline S. Foo<sup>d</sup>, Cheng Liu<sup>b</sup>, Suping Ren<sup>b</sup>, Leonid Beigelman<sup>a,b</sup>, Lawrence M. Blatt<sup>a,b</sup>, Sandro Boland<sup>e</sup>, Laura Vangeel<sup>d</sup>, Steven Dejonghe<sup>d</sup>, Patrick Chaltin<sup>c,e</sup>, Arnaud Marchand<sup>e</sup>, Vladimir Serebryany<sup>b</sup>, Antitsa Stoycheva<sup>b</sup>, Sushmita Chanda<sup>b</sup>, Julian A. Symons<sup>b</sup>, Pierre Rabisson<sup>a</sup>, Johan Neyts<sup>d,\*\*</sup>

<sup>a</sup> Aligos Belgium BV, Gaston Geenslaan 1, 3001 Leuven, Belgium

<sup>b</sup> Aligos Therapeutics, Inc., 1 Corporate Dr., 2nd Floor, South San Francisco, CA, USA

<sup>c</sup> Centre for Drug Design and Discovery (CD3), KU Leuven, Gaston Geenslaan 2, 3001 Leuven, Belgium

<sup>d</sup> Rega Institute for Medical Research, KU Leuven, Herestraat 49, 3000 Leuven, Belgium

<sup>e</sup> CISTIM Leuven vzw, Gaston Geenslaan 2, 3001 Leuven, Belgium

### ARTICLE INFO

#### Article history:

Received 14 February 2021

Accepted 18 March 2021

Available online 26 March 2021

#### Keywords:

COVID-19

Coronavirus

3CLpro

Protease inhibitor

### ABSTRACT

There is an urgent need for antivirals targeting the SARS-CoV-2 virus to fight the current COVID-19 pandemic. The SARS-CoV-2 main protease (3CLpro) represents a promising target for antiviral therapy. The lack of selectivity for some of the reported 3CLpro inhibitors, specifically versus cathepsin L, raises potential safety and efficacy concerns. ALG-097111 potently inhibited SARS-CoV-2 3CLpro ( $IC_{50} = 7$  nM) without affecting the activity of human cathepsin L ( $IC_{50} > 10$   $\mu$ M). When ALG-097111 was dosed in hamsters challenged with SARS-CoV-2, a robust and significant  $3.5 \log_{10}$  (RNA copies/mg) reduction of the viral RNA copies and  $3.7 \log_{10}$  (TCID<sub>50</sub>/mg) reduction in the infectious virus titers in the lungs was observed. These results provide the first *in vivo* validation for the SARS-CoV-2 3CLpro as a promising therapeutic target for selective small molecule inhibitors.

© 2021 Elsevier Inc. All rights reserved.

### 1. Introduction

Inhibition of the HCV and HIV viral proteases with antiviral drugs is a proven successful therapeutic approach [1]. With the continuing global COVID-19 pandemic and the urgent need for effective SARS-CoV-2 antivirals, investigators have repurposed previously discovered antiviral drugs initially designed against other viruses. These efforts have resulted in the approval of remdesivir, a nucleotide analogue inhibiting the nsp12 polymerase, previously developed for Ebola [2,3]. A second nsp12 inhibitor, MK-

4482/EIDD-2801, is currently being evaluated in the clinic [4,5]. The SARS-CoV-2 main protease (Mpro, 3CLpro) represents another promising target for antiviral therapy with no human homologue. Currently, the most advanced drug candidate targeting the SARS-CoV-2 3CLpro, is PF-07304814, a phosphate prodrug of PF-00835231 [6], discovered more than 15 years ago in the context of the SARS-CoV-1 outbreak [7]. Since the initial SARS-CoV-2 outbreak, several reports of 3CLpro inhibitors with *in vitro* potency against SARS-CoV-2 have been reported [8]. However, the lack of selectivity of some of these compounds, specifically versus cathepsin L, raises questions on the overestimation of the 3CLpro component of *in vitro* cellular potency and its translation towards *in vivo* activity [9]. Cathepsin L is involved in the entry of SARS-CoV-2 into host cells and therefore contributes to non-selective 3CLpro inhibitor potency in commonly used cell lines. GC-376, a broad spectrum inhibitor of 3C, 3C-like proteases and cathepsin L,

\* Corresponding author.

\*\* Corresponding author.

E-mail addresses: [kvandyck@aligos.com](mailto:kvandyck@aligos.com) (K. Vanduyck), [johan.neyts@kuleuven.be](mailto:johan.neyts@kuleuven.be) (J. Neyts).

failed to show a clear antiviral effect in monotherapy in a mouse model of SARS-CoV-2 infection [10]. In another study modest antiviral activity was observed in the K18-hACE2 SARS-CoV-2 infection mouse model [11]. Until now the SARS-CoV-2 3CLpro remains to be validated as a promising therapeutic target; which is only possible with a 3CLpro inhibitor that lacks activity against other proteases such as cathepsin L. We applied a structure-based strategy with early monitoring of cathepsin L inhibition in parallel with SARS-CoV-2 3CLpro inhibition. As a result, we identified ALG-097111, a potent and selective SARS-CoV-2 3CLpro inhibitor, which has demonstrated proof of concept by inhibiting SARS-CoV-2 infection in an in vivo SARS-CoV-2 hamster model.

## 2. Materials and methods

### 2.1. SARS-CoV-2 3CLpro and human cathepsin L biochemical assays

The SARS-CoV-2 3CLpro and human cathepsin L assays were performed as previously described [12].

### 2.2. Human $\beta$ -coronavirus OC43 assay

The human beta-coronavirus OC43 assay in HeLa cells was performed as previously described [13].

### 2.3. Human $\alpha$ -coronavirus 229E assay

The human alpha-coronavirus 229E was purchased from Virapur (San Diego, CA) and propagated using MRC-5 human lung fibroblast cells (ATCC). Huh7 cells (JCRB cell Bank) were cultured using DMEM media, supplemented with 10% fetal bovine serum (FBS), 1% (v/v) penicillin/streptomycin (P/S), 1% (v/v) HEPES and 1% (v/v) cellgro glutagro™ supplement (all Corning, Manassas, VA) at 37 °C.  $1.5 \times 10^4$  Huh7 cells per well were cultured for 24 h prior to infection. Then, serially diluted compounds in assay media (DMEM, 4% FBS, 1% P/S, 1% cellgro glutagro™ supplement, 1% HEPES) were added to the cells and incubated for 4 h at 37 °C. The 229E virus stock was diluted to a concentration known to produce optimal cytopathic effect and was added to cells in 96-well plates that were then incubated for 4 days at 33 °C. Cellular cytotoxicity plates without the addition of 229E virus were set up in parallel. At the end of the incubation period, 100  $\mu$ l of cell culture supernatant was replaced with 100  $\mu$ l CellTiter-Glo® (Promega, Madison, WI) and incubated for at least 10 min at room temperature prior to measuring luminescence on a PerkinElmer (Waltham, MA) Envision plate reader.

### 2.4. SARS-CoV-2 nanoluciferase assay in human ACE-2 expressing A549 cells

The SARS-CoV-2 nanoluciferase assay using A549 cells expressing the human ACE-2 receptor was performed in the laboratory of Pei-Yong Shi at the University of Texas, Medical Branch [14] on behalf of Aligos Therapeutics, Inc. Cytotoxicity was assessed on A549 cells (Sigma) that were maintained in F12 Media, supplemented with 10% fetal bovine serum (FBS), 1% (v/v) penicillin/streptomycin (P/S), 1% (v/v) HEPES and 1% (v/v) cellgro glutagro™ supplement at 37 °C with 5% CO<sub>2</sub>.  $1.2 \times 10^4$  A549 cells per well were plated in 96-well plates and cultured for up to 24h. Compounds were diluted in F12 Media containing low FBS (2%) and added to cells and incubated for 48 h. Reduction of cell viability was measured as described above.

## 2.5. Compounds

Ritonavir was purchased from Fluorochem (CAS 155213-675, FCC3125867). EIDD-2801 was purchased from Excenen Pharmatech Co., Ltd. GS-441524 (parent nucleoside of remdesivir) was obtained from Carbosynth (cat no AG167808). Compounds in Table 1 were prepared via methodologies described in the literature [6,15–19].

### 2.6. SARS-CoV-2 infection model in primary human lung epithelial cells

Human small airway epithelia cell cultures were derived from a healthy donor and differentiated in an air-liquid culture system and as such obtained from Epithelix (cat no EP21SA). Cultures were maintained as described by the manufacturer before use. At the start of the experiment the apical side of the cultures were washed once with PBS and the inserts were transferred to wells containing the appropriate compound concentration in basal medium (SmallAir culture medium Epithelix). After 1.5 h incubation at (35 °C, 5%CO<sub>2</sub>) the inserts were infected by adding SARS-CoV-2-GHB-03021/2020 at  $2 \times 10^4$  TCID<sub>50</sub> in 100  $\mu$ l of PBS at the apical side. After 2 h incubation the virus inoculum was removed and the inserts were further incubated (35 °C, 5%CO<sub>2</sub>). The basal medium (with or without compound) was replaced every two days. Virus production at the apical side was determined on day 1, 2, 4 and 6 by washing this side with 100  $\mu$ l PBS and quantification of the amount of vRNA by first mixing 5  $\mu$ l wash fluid with 50  $\mu$ l Cells-to-cDNA II Cell Lysis Buffer (ThermoFisher) and heating at 75 °C or 15 min. The samples were subsequently diluted by adding 150  $\mu$ l of water and 4  $\mu$ l was used for RT-qPCR performed on a LightCycler96 platform (Roche) using the iTaq Universal Probes One-Step RT-qPCR kit (BioRad) with N1 primers and probes targeting the nucleocapsid (IDTDNA, cat no 10006770). Standards for the RT-qPCR were prepared by a 10-fold dilution of SARS-CoV-2-GHB-03021/2020 virus stock with known infectivity and using this in the same extraction/amplification protocol. The amount of vRNA in the samples could be calculated to TCID<sub>50</sub> equivalents.

### 2.7. SARS-CoV-2 infection model in hamsters

The hamster infection model of SARS-CoV-2, the SARS-CoV-2 isolate, SARS-CoV-2 RT-qPCR and End-point virus titrations has been described previously [20,21].

### 2.8. Treatment regimen

Female hamsters, 6–8 weeks old were anesthetized with ketamine/xylazine/atropine and inoculated intranasally with 50  $\mu$ l containing  $2 \times 10^6$  TCID<sub>50</sub> SARS-CoV-2-GHB-03021/2020 (day 0). Beginning 2 h before infection, animals were treated twice daily with either vehicle used for ALG-097111 (60% PEG400 in water, subcutaneous[SC]) + ritonavir (50 mg/kg/dose, BID oral gavage) [negative control group] or ALG-097111 (200 mg/kg/dose, BID, SC) + ritonavir (50 mg/kg/dose, BID, oral gavage) or EIDD-2801 (200 mg/kg/dose, oral gavage as a positive control). Hamsters were monitored for appearance, behavior and weight. At day 2 post infection (pi) (day 3), 6 h following the 5th dose, hamsters were euthanized by IP injection of 500  $\mu$ l Dolethal (200 mg/mL sodium pentobarbital, Vétquinol SA). Lungs were collected and viral RNA and infectious virus were quantified by RT-qPCR and end-point virus titration, respectively.

## 2.9. Pharmacokinetics (PK) analysis of ALG-097111 in plasma and lung

### 2.9.1. Animal and treatments for PK evaluations

Male Sprague Dawley rats were group-housed during acclimation and in-life portions of the study. The animal room environment was controlled and monitored daily with target temperature 20–26 °C, relative humidity 30–70%, 12 h artificial light and 12 h dark. All animals had access to certified rodent diet and reverse-osmosis water ad libitum. Animals were deprived of food overnight prior to dosing (fasted within 14 h of dosing) and fed immediately after the 4-h timepoint collection.

For the intravenous administration at 2 mg/kg, ALG-097111 was dissolved in 80% PEG400 in water. For the single dose administration via oral gavage at 10 mg/kg, ALG-097111 was dissolved in 40% PEG400 in water and dosed at 5 mL/kg. The formulation for subcutaneous administration at 50 mg/kg was 40% PEG400 in water. The blood collection in K<sub>2</sub>EDTA containing tubes was conducted at multiple timepoints from 0.083 to 24-h postdose from both PO and SC dosed animals. The samples were kept cold on wet ice until centrifugation to harvest plasma.

Female golden Syrian hamsters were group-housed during acclimatization and in-life portions of the study. The animal room environment was controlled for temperature, humidity, and light/dark cycle as described for rats. All animals had access to certified rodent diet and reverse-osmosis water ad libitum. The animals were dosed 10 h apart subcutaneously with 200 mg/kg/dose BID of ALG-097111 in 60% PEG400 in water. An oral gavage dose of ritonavir at 50 mg/kg in 95% PEG400 and 5% copovidone was administered just prior to each subcutaneous dose of ALG-097111. Blood samples at multiple timepoints from 0.25- to 24-h postdose were collected into tubes containing K<sub>2</sub>EDTA and kept on ice until processing to harvest plasma. Lung samples were collected at 24 h after the first dose, flash frozen on dry ice and stored at ≤70 °C until processing and analysis, then homogenized with methanol-water (7:3) on wet ice. The homogenate was centrifuged, and the supernatant was used for bioanalysis.

All *in vivo* studies were approved by the IACUC at their respective institutions

### 2.9.2. Bioanalysis of plasma and lung extract

The samples were analyzed by LC-MS/MS method using ACQUITY UPLC system (Waters Corporation, Milford, MA) and Sciex Triple Quad™ 6500+ LC-MS/MS System. The plasma samples processed by protein precipitation method were injected on ACQUITY UPLC BEH C18 1.7 μm 2.1 × 50 mm column. A gradient of 0.1% formic acid in water and acetonitrile at 0.6 mL/min was used. The mass spectrum was operated in positive ionization mode.

### 2.9.3. *In vitro* stability in microsomes and hepatocytes

Stability studies with ALG-097111 at 1 μM were performed in hamster, dog and human liver microsomes, and in dog and human hepatocytes. Details can be found in the supplementary information.

## 2.10. Secondary *in vitro* pharmacology

ALG-097111 was profiled up to a concentration of 10 μM in the safety 44 CEREP panel, a panel of receptor, enzyme and uptake assays (44 total) and on a panel of 58 kinases. ALG-097111 was tested on a set of 9 proteases (Calpain 1, Caspase 2, Cathepsin B, Cathepsin D, Cathepsin L, Chymotrypsin, Elastase, Thrombin a, and Trypsin).

## 3. Results and discussion

The entry of SARS-CoV-2 into the target cells is a process that can be mediated by multiple proteases including cysteine cathepsins B and L or the transmembrane protease serine 2 (TMPRSS2) [22,23]. The cathepsin L inhibitor K117777, which lacks an inhibitory effect on the 3CLpro results in potent inhibition of SARS-CoV-2 in VeroE6, A549-ACE2 and HeLa-ACE2 [24].

Although lung tissue cells express both cathepsins and TMPRSS2, many cell-lines commonly used for screening, such as A549, lack TMPRSS2 [9]. Strikingly, the potent antiviral effect of K117777 was abolished when TMPRSS2 was expressed in A549-ACE2. Off target activity of 3CLpro inhibitors could lead to an inaccurate assessment of the potential activity of a lead candidate *in vivo*. Indeed, the antiviral potency in cell-based assays will be overestimated when tested on cell lines not reproducing all entry pathways. Moreover, these non-selective inhibitors will have to compete *in vivo* for viral and host enzymes, likely leading to a further reduction of the antiviral potency. In addition, cysteine cathepsins are key regulators of both the innate and adaptive immunity to pathogens [25,26]. In particular, Cathepsin L primes T-cells by processing the antigens in the lysosomal compartment of Antigen Presenting Cells (APC's), by presenting the proteolytic degradation peptides on the MHC class II [27], processing the MHC class II [28] and different Toll-like receptors (TLR3, -7 and -9) [29,30] and by controlling the secretion of different cytokines [25,26]. Therefore, 3CLpro inhibitors that lack selectivity toward cathepsin L, may potentially have counter-effective side effects by dampening the immune response against SARS-CoV-2 [31]. This may be expected to aggravate the already impaired T-cell immunity of COVID-19 patients who often suffer from lymphocytopenia, reduced expression of MHCII and pro-inflammatory cytokines.

The selectivity of a set of reported SARS-CoV-2 3CLpro inhibitors versus cathepsin L, was assessed in a biochemical assay (Table 1). The examples depicted indicate that mimicking the substrates glutamine in P1 of the inhibitor, is not sufficient to obtain a selective inhibitor against the 3CL protease and that Cathepsin L tolerates this substituent, resulting in potent inhibition.

### 3.1. *In vitro* profiling of ALG-097111

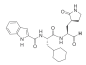
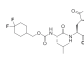
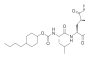
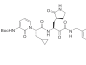
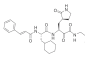
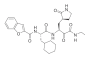
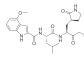
Structure-based optimization, combined with cathepsin L and SARS-CoV-2 3CLpro biochemical activities, resulted in the discovery of the selective 3CLpro inhibitor ALG-097111. In biochemical assays, ALG-097111 potently inhibited SARS-CoV-2 3CLpro (IC<sub>50</sub> = 7 nM, n = 5) without affecting the activity of human cathepsin L (IC<sub>50</sub> > 10 μM, n = 3) (Figure S1). The selectivity of ALG-097111 was confirmed by *in vitro* testing of a panel of 44 receptors, 58 kinases (no inhibition was noted up to 10 μM) and 9 human proteases (<50% inhibition at 10 μM).

In comparison, GC376 and PF-00835231 were significantly less selective against human cathepsin L. ALG-097111 inhibited replication of SARS-CoV-2 in A549 cells expressing the human ACE-2 receptor with an EC<sub>50</sub> of 200 ± 18.4 nM (n = 2). No cytotoxicity was observed in A549 cells at concentrations up to 100 μM, resulting in an *in vitro* selectivity of over 500. The activity of ALG-097111 extended to other human coronaviruses such as the alpha-coronavirus 229E and the beta-coronavirus OC43, demonstrating broad-spectrum anti-coronaviral activity. (Table 2).

The anti-SARS-CoV-2 activity of ALG-097111 was confirmed in human small airway epithelial cell cultures derived from a healthy donor and differentiated in an air-liquid culture system (Figure S2). When ALG-097111 was added at a concentration of 1 μM to the basolateral side of the cultures, the compound reduced viral RNA yield in the washes at the apical site of the culture by > 3 log<sub>10</sub>.

**Table 1**

Overview of a set of reference compounds and their inhibitory potency on Cathepsin L and SARS-CoV-2 3CLpro in a biochemical assay.

							
Cathepsin L IC <sub>50</sub> (nM)	Cpd 11a [15] 0.21 (n = 2)	6j [16] <0.5 (n = 2)	6e [16] <0.5 (n = 2)	Cpd 13b [17] 291 (n = 2)	Cpd 11r [18] <0.5 (n = 2)	A9 [19] <0.5 (n = 2)	PF-231 [6] 146 (n = 13)
SARS-CoV-2 3CLpro IC <sub>50</sub> (nM)	8 (n = 28)	7 (n = 2)	10 (n = 3)	472 (n = 2)	1154 (n = 2)	4891 (n = 2)	5 (n = 5)

**Table 2**

Antiviral activity and cytotoxicity of ALG-097111, and remdesivir in various cell-based antiviral assays.

	SARS-CoV-2Nluc (A549) <sup>a</sup>		β-CoV OC43 (HeLa)		α-CoV 229E (Huh-7)	
	EC <sub>50</sub> [nM]	CC <sub>50</sub> [nM]	EC <sub>50</sub> [nM]	CC <sub>50</sub> [nM]	EC <sub>50</sub> [nM]	CC <sub>50</sub> [nM]
ALG-097111	200 ± 18.4 (n = 2)	>100 000	123.3 ± 21.1 (n = 4)	>100 000	366.5 ± 199.1 (n = 2)	>25 000
Remdesivir	31.6 ± 11.9 (n = 2)	>50 000	102.4 ± 50.53 (n = 46)	>5000	14.47 ± 3.48 (n = 18)	>1000

<sup>a</sup> The SARS-CoV-2-Nluc antiviral assay was performed using A549-hACE2 cells while the cytotoxicity was performed in A549 cells.

While ALG-097111 is stable in human and dog liver microsomes ( $t_{1/2}$  >60 min) and hepatocytes ( $t_{1/2}$  >360 min), it has a lower stability in hamster liver microsomes ( $t_{1/2}$  = 15 min). In the presence of ritonavir ( $\mu$ M), the *in vitro* half-life in hamster liver microsomes increased ( $t_{1/2}$  = > 60 min).

### 3.2. *In vivo* pharmacokinetic evaluation of ALG-097111

ALG-097111 displayed low clearance (11.2 mL/min/kg), moderate volume of distribution (0.79 L/kg) and half-life of 2.0 h following a single intravenous dose at 2 mg/kg in rats. Plasma PK profile of ALG-097111 in rats was obtained following a single dose at 10 mg/kg administered via oral gavage and at 50 mg/kg via subcutaneous injection. Although, the bioavailability following the oral dose was low (3.2%). The systemic exposure following the subcutaneous administration was significantly higher with bioavailability of 44%. The comparative plasma profile is depicted in Fig. 1A.

When ALG-097111 was co-administered in female hamsters at 200 mg/kg/dose BID with ritonavir given PO at 50 mg/kg/dose BID, the plasma and lung C<sub>trough</sub> of 1105 nM and 611 nM, were 5.5 and 3.0-fold above the *in vitro* EC<sub>50</sub> on SARS-CoV-2 in A549, respectively. The hamster plasma PK profile and lung concentration at 24 h are shown in Fig. 1B.

### 3.3. Evaluation of *in vivo* efficacy of ALG-097111 in SARS-CoV-2 infected Syrian hamsters

The high *in vitro* efficacy of the compound for inhibiting SARS-CoV-2 virus combined with its *in vitro* metabolic stability in non-rodents and human matrices and PK profile in rat led to selection of

the compound for *in vivo* evaluation of its efficacy. The *in vivo* anti-SARS-CoV-2 efficacy of ALG-097111 was evaluated in female SG hamsters dosed twice daily with 200 mg/kg of ALG-097111 in combination with ritonavir (50 mg/kg/dose). Other hamsters were treated orally BID with the vehicle + ritonavir (i.e. the control group) or molnupiravir (EIDD-2801) (200 mg/kg as a positive control group). All animals received 5 administrations in total, starting 2 h before infection. At day 2 pi, the animals were euthanized, and lungs were collected for quantification of viral loads. Treatment of infected hamsters with ALG-097111 resulted in 3.5 log<sub>10</sub> reduction in the viral RNA copies per mg of lung tissue ( $P$  = 0.008) as compared to the vehicle/ritonavir-treated animals (Fig. 2A). In hamsters that had been treated with 200 mg/kg BID of molnupiravir (EIDD-2801) a 2.0 log<sub>10</sub> reduction in the viral RNA copies/mg of lung tissue was noted ( $P$  = 0.095, non-significant) (Fig. 2A). Both compounds significantly reduced the infectious virus titers in the lungs by 3.7 ( $P$  = 0.008) and 4.1 ( $P$  = 0.008) log<sub>10</sub> TCID<sub>50</sub> per mg for ALG-097111 and EIDD-2801, respectively (Fig. 2B).

In conclusion, ALG-097111, a selective SARS-CoV-2 3CLpro inhibitor, is a potent inhibitor of the *in vitro* replication of SARS-CoV-2 and efficiently inhibits viral replication in the lungs of infected hamsters. To the best of our knowledge, this is the first time that a selective SARS-CoV-2 3CLpro inhibitor (i.e. without a significant inhibitory effect on cathepsin L activity), has been shown to result in such a pronounced inhibitory effect on SARS-CoV-2 replication in an animal infection model. Future studies will focus on combinations with other modalities against SARS-CoV-2, as well as investigation of compound dosing in a therapeutic setting.

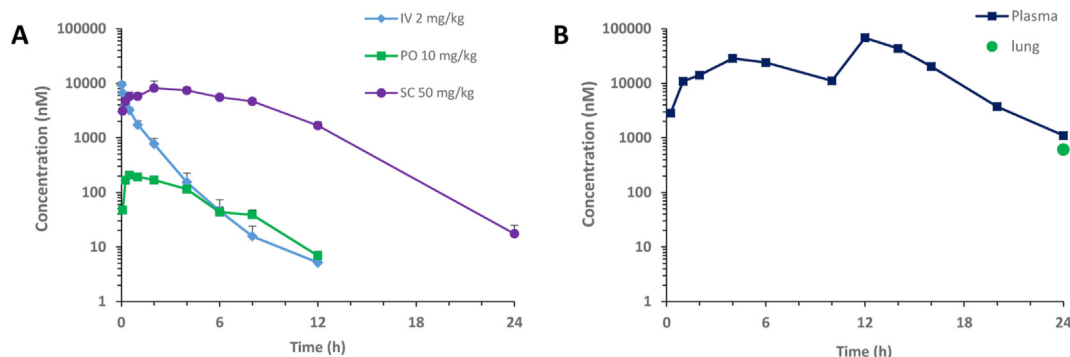


**Fig. 1.** A) Plasma PK of ALG-097111 in male Sprague Dawley rats following a single IV, PO or SC dose. B) Plasma PK profile and lung concentration at 24 h of ALG-097111 in female golden Syrian hamsters following BID administration of ritonavir given orally at 50 mg/kg/BID prior to ALG-097111 given subcutaneously at 200 mg/kg/dose.



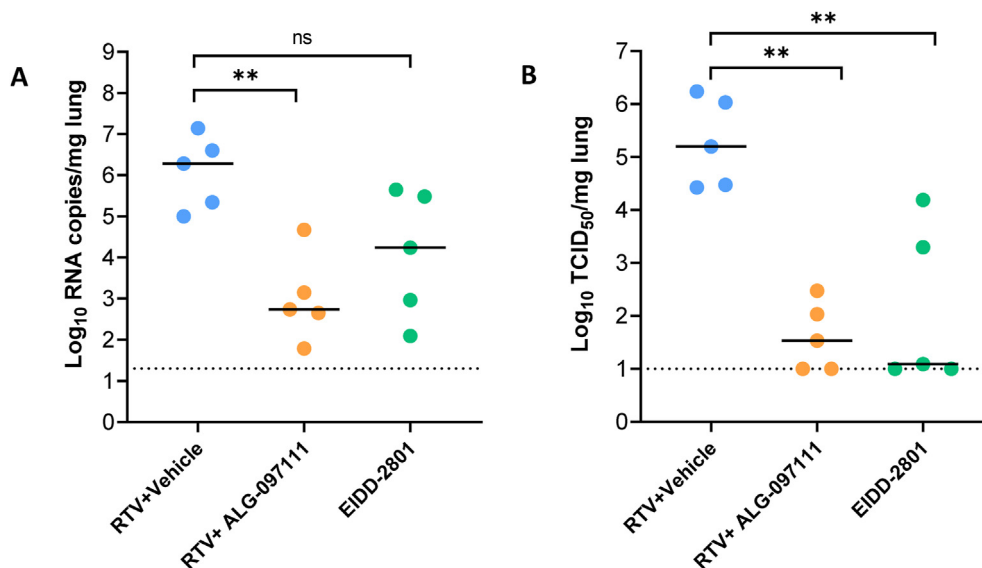


**Fig. 2.** *In vivo* efficacy of ALG-097111 against SARS-CoV-2 in SG hamsters. (A) Viral RNA levels in the lungs of ritonavir (PO)+vehicle (SC) (50 + 0 mg/kg/dose, BID), ritonavir (PO)+ALG-097111 SC (50 + 200 mg/kg/dose, BID, SC) and EIDD-2801-PO (200 mg/kg/dose, BID) SARS-CoV-2-infected hamsters at day 2 post-infection (pi) are expressed as log<sub>10</sub> SARS-CoV-2 RNA copies per mg lung tissue. Individual data and median values are presented. (B) Infectious viral loads in the lungs of ritonavir (PO)+vehicle SC (50 + 0 mg/kg/dose, BID), ritonavir (PO) +ALG-097111 SC (50 + 200 mg/kg/dose, BID) and EIDD-280 (PO) (200 mg/kg/dose, BID) SARS-CoV-2-infected hamsters at day 2 post-infection (pi) are expressed as log<sub>10</sub> TCID<sub>50</sub> per mg lung tissue. Individual data and median values are presented. Data were analyzed with the Mann–Whitney *U* test. \*\**P* < 0.01, ns = non-significant. RTV = ritonavir.

## Acknowledgments

We thank Carolien De Keyser, Lindsey Bervoets, Thibault Francken, Birgit Voeten, Niels Cremers, Tina Van Buyten, Joost Schepers, Winston Chiu and Kim Donckers for excellent technical assistance. We are grateful to Piet Maes for kindly providing the SARS-CoV-2 strain used in this study. A special thanks to Dr Hongjie Xia in the laboratory of Prof Dr Pei-Yong Shi at the University of Texas Medical Branch for kindly performing the SARS-CoV-2 Nanoluc antiviral assay.

## Appendix A. Supplementary data

Supplementary data related to this article can be found at <https://doi.org/10.1016/j.bbrc.2021.03.096>.

## Declaration of competing interests

The authors declare the following financial interests/personal relationships which may be considered as potential competing interests:

Koen Vandyck and Pierre Raboisson are employees of Aligos Belgium BV

Kusum Gupta, Andreas Jekle, Jerome Deval, Dinah Misner, Cheng Liu, Suping Ren, Leonid Beigelman, Lawrence M. Blatt, Vladimir Serebryany, Antitsa Stoycheva, Sushmita Chanda, Julian A. Symons are employees of Aligos Therapeutics, Inc.

A patent application on ALG-097111 is pending

## References

- [1] A.A. Agbowuro, et al., Proteases and protease inhibitors in infectious diseases, *Med. Res. Rev.* 38 (2018) 1295–1331, <https://doi.org/10.1002/med.21475>.
- [2] W. Zhu, et al., RNA-dependent RNA polymerase as a target for COVID-19 drug discovery, *SLAS DISCOVERY: Advancing the Science of Drug Discovery* 25 (2020) 1141–1151, <https://doi.org/10.1177/247255220942123>.
- [3] Y. Wang, et al., Remdesivir in adults with severe COVID-19: a randomised, double-blind, placebo-controlled, multicentre trial, *Lancet* 395 (2020) 1569–1578, [https://doi.org/10.1016/S0140-6736\(20\)31022-9](https://doi.org/10.1016/S0140-6736(20)31022-9).
- [4] Efficacy and safety of molnupiravir (MK-4482) in hospitalized adult participants with COVID-19 (MK-4482-001). <https://ClinicalTrials.gov/show/NCT04575584>.
- [5] Efficacy and safety of molnupiravir (MK-4482) in non-hospitalized adult participants with COVID-19 (MK-4482-002). <https://ClinicalTrials.gov/show/NCT04575597>.
- [6] R.L. Hoffman, et al., Discovery of ketone-based covalent inhibitors of coronavirus 3CL proteases for the potential therapeutic treatment of COVID-19, *J. Med. Chem.* 63 (2020) 12725–12747, <https://doi.org/10.1021/acs.jmedchem.0c01063>.
- [7] L. Hoffman Robert, et al., Anticoronaviral Compounds and Compositions, Their Pharmaceutical Uses And Materials For Their Synthesis, Pfizer, WO2005113580.
- [8] C.-C. Chen, et al., Overview of antiviral drug candidates targeting coronaviral 3C-like main proteases, *FEBS J.* (2021), <https://doi.org/10.1111/febs.15696> n/a.
- [9] K. Steuten, et al., Challenges for targeting SARS-CoV-2 proteases as a therapeutic strategy for COVID-19, *bioRxiv* (2020), <https://doi.org/10.1101/2020.11.21.392753>, 2020.2011.2021.392753.
- [10] Y. Shi, et al., The preclinical inhibitor GS441524 in combination with GC376 efficaciously inhibited the proliferation of SARS-CoV-2 in the mouse respiratory tract, *bioRxiv* (2020), <https://doi.org/10.1101/2020.11.12.380931>, 2020.2011.2012.380931.
- [11] C. Joaquín Cáceres, et al., Efficacy of GC-376 against SARS-CoV-2 virus infection in the K18 hACE2 transgenic mouse model, *bioRxiv* (2021), <https://doi.org/10.1101/2021.01.27.428428>, 2021.2001.2021.428428.
- [12] C. Liu, et al., Dual inhibition of SARS-CoV-2 and human rhinovirus with protease inhibitors in clinical development, *Antivir. Res.* 187 (2021) 105020, <https://doi.org/10.1016/j.antiviral.2021.105020>.
- [13] Z.A. Gurard-Levin, et al., Evaluation of SARS-CoV-2 3C-like protease inhibitors using self-assembled monolayer desorption ionization mass spectrometry, *Antivir. Res.* 182 (2020) 104924, <https://doi.org/10.1016/j.antiviral.2020.104924>.
- [14] X. Xie, et al., A nanoluciferase SARS-CoV-2 for rapid neutralization testing and screening of anti-infective drugs for COVID-19, *Nat. Commun.* 11 (2020) 5214, <https://doi.org/10.1038/s41467-020-19055-7>.
- [15] W. Dai, et al., Structure-based design of antiviral drug candidates targeting the SARS-CoV-2 main protease, *Science* 368 (2020) 1331, <https://doi.org/10.1126/science.abb4489>.
- [16] A.D. Rathnayake, et al., 3C-like protease inhibitors block coronavirus replication in vitro and improve survival in MERS-CoV-infected mice, *Sci. Transl. Med.* 12 (2020), <https://doi.org/10.1126/scitranslmed.abc5332> eabc5332.
- [17] L. Zhang, et al., Crystal structure of SARS-CoV-2 main protease provides a basis for design of improved  $\alpha$ -ketoamide inhibitors, *Science* 368 (2020) 409, <https://doi.org/10.1126/science.abb3405>.
- [18] L. Zhang, et al.,  $\alpha$ -Ketoamides as broad-spectrum inhibitors of coronavirus and enterovirus replication: structure-based design, synthesis, and activity assessment, *J. Med. Chem.* 63 (2020) 4562–4578, <https://doi.org/10.1021/acs.jmedchem.9b01828>.

- [19] H. Liu, et al., Ketoamide Compound and Preparation Method, Pharmaceutical Composition, and Use Thereof, Shanghai Inst Materia Medica ; univ fudan, WO2020030143.
- [20] R. Boudewijns, et al., STAT2 signaling restricts viral dissemination but drives severe pneumonia in SARS-CoV-2 infected hamsters, *Nat. Commun.* 11 (2020) 5838, <https://doi.org/10.1038/s41467-020-19684-y>.
- [21] S.J.F. Kaptein, et al., Favipiravir at high doses has potent antiviral activity in SARS-CoV-2-infected hamsters, whereas hydroxychloroquine lacks activity, in: *Proceedings of the National Academy of Sciences*, vol. 117, 2020, p. 26955, <https://doi.org/10.1073/pnas.2014441117>.
- [22] J. Shang, et al., Cell entry mechanisms of SARS-CoV-2, in: *Proceedings of the National Academy of Sciences*, vol. 117, 2020, p. 11727, <https://doi.org/10.1073/pnas.2003138117>.
- [23] M. Hoffmann, et al., SARS-CoV-2 cell entry depends on ACE2 and TMPRSS2 and is blocked by a clinically proven protease inhibitor, *Cell* 181 (2020) 271–280, <https://doi.org/10.1016/j.cell.2020.02.052>, e278.
- [24] D.M. Mellott, et al., A cysteine protease inhibitor blocks SARS-CoV-2 infection of human and monkey cells, *bioRxiv* (2020), <https://doi.org/10.1101/2020.10.23.347534>, 2020.10.23.347534.
- [25] P.I. Bird, et al., Endolysosomal proteases and their inhibitors in immunity, *Nat. Rev. Immunol.* 9 (2009) 871–882, <https://doi.org/10.1038/nri2671>.
- [26] T. Jakoš, et al., Cysteine cathepsins in tumor-associated immune cells, *Front. Immunol.* 10 (2019), <https://doi.org/10.3389/fimmu.2019.02037>.
- [27] J.D. Colbert, et al., Diverse regulatory roles for lysosomal proteases in the immune response, *Eur. J. Immunol.* 39 (2009) 2955–2965, <https://doi.org/10.1002/eji.200939650>.
- [28] T. Yadati, et al., The ins and outs of cathepsins: physiological function and role in disease management, *Cells* 9 (2020), <https://doi.org/10.3390/cells9071679>.
- [29] S.E. Ewald, et al., Nucleic acid recognition by Toll-like receptors is coupled to stepwise processing by cathepsins and asparagine endopeptidase, *J. Exp. Med.* 208 (2011) 643–651, <https://doi.org/10.1084/jem.20100682>.
- [30] A. Garcia-Cattaneo, et al., Cleavage of Toll-like receptor 3 by cathepsins B and H is essential for signaling, in: *Proceedings of the National Academy of Sciences*, vol. 109, 2012, p. 9053, <https://doi.org/10.1073/pnas.1115091109>.
- [31] M.V. Baranov, et al., The PIKfyve inhibitor apilimod: a double-edged sword against COVID-19, *Cells* 10 (2021), <https://doi.org/10.3390/cells10010030>.